Photoinduced Cytotoxicity and Biodistribution of Prostate Cancer Cell-Targeted Porphyrins

Inder Sehgal,* Martha Sibrian-Vazquez, and M. Graça H. Vicente

Department of Comparative Biomedical Sciences and Department of Chemistry, Louisiana State University, Baton Rouge Louisiana 70803

Received April 18, 2008

A series of five porphyrin−peptide conjugates bearing one or two sequences containing a cell penetrating peptide (CPP), a nuclear localization signal (NLS), or a bifunctional CPP-NLS or NLS-CPP sequences were synthesized and investigated in vitro using PC-3M human prostate cancer cells, in comparison with FDA-approved purified hematoporphyrin derivative (Porfimer Sodium) and mTHPC. The most promising porphyrin−HIV-1 Tat (48−60) conjugate **2** [lowest dark cytotoxicity ($IC_{50} = 38.0\ \mu M$), highest phototoxicity ($IC_{50} = 0.40\ \mu M$ at 1 J/cm^2)] was further evaluated in an in vivo biodistribution study using SCID mice bearing PC-3M tumors, in comparison with purified hematoporphyrin derivative. Porphyrin conjugate **2** was more tumor selective than the hematoporphyrin derivative and accumulated to a significantly greater extent in tumors. Our results show that effective photodynamic cytotoxicity can be induced in human prostate cancer cells with minimal dark toxicity and that selective accumulation in prostate tumors can be achieved in vivo with porphyrin-targeted photosensitizers.

1. Introduction

Porphyrin-type compounds constitute a major class of pharmacological agents under investigation for application in the early diagnosis and treatment of cancer by photodynamic therapy (PDT) and a variety of other diseases. Two porphyrin derivatives, purified hematoporphyrin derivative (Porfimer Sodium sold as Photofrin) and verteporfin, are FDA-approved for the PDT treatment of melanoma, early and advanced stage cancer of the lung, digestive tract, genitourinary tract, and the wet form of age-related macular degeneration, respectively.[1,2] Both of these drugs are mixtures of compounds with limited specificity for tumor tissue. Although both drugs have been successfully used to treat several thousands of patients worldwide, skin photosensitivity is often an undesirable side effect in purified hematoporphyrin derivative PDT due to prolonged retention of this drug in patients skin. This unwanted side effect has been minimized or eliminated with the use of second-generation PDT photosensitizers (e.g., HPPH, motexafin lutetium, monoaspartylchlorin e6, mTHPC, Pd-bacteriopheophorbide) currently undergoing clinical investigations.[3] Prostate cancer is the most common internal malignancy in the U.S. Most cases are organ confined and are presently treated by either surgery, external beam radiation, or brachytherapies.[4] Until recently, PDT was not a viable alternative for prostate cancer treatment due to the limited tissue penetration ability of the laser wavelengths normally used in PDT and the poor tumor selectivity of the currently available photosensitizers.[4,5] However, the development of drugs photoactivated in the infrared region coupled with the use of optical fibers inserted transperineally into the prostate have allowed efficient interstitial light delivery. These optical fibers allow laser exposure of the entire gland.[4,6]

On the basis of these advances, a limited number of clinical trials using PDT against human prostate cancer have been performed. Three have involved the use of PDT against disease in men who have had local recurrence following external beam radiation.[4,6,7] Traditional treatment options for these men include prostatectomy, cryosurgery, or further radiation.[4] In these studies, PDT was successfully delivered, produced little or no lasting incontinence or erectile dysfunction, induced necrosis in the tumor sites, and reduced PSA levels. In addition, at least one trial utilized PDT as the initial treatment of organ-confined prostate cancer; in this trial, mTHPC was used, and it also induced necrosis, decreased PSA levels, and left patients with little incontinence and erectile dysfunction.[8] Thus PDT is a developing option for patients who choose a minimally invasive procedure.[4,6,8] However, a major drawback of mTHPC as well as other currently known photosensitizers is their poor selectivity for prostate tumors.[8] Therefore, a major goal for prostate cancer PDT is to develop photosensitizing agents with greater tumor selectivity and more favorable tumor to nontumor tissue biodistribution.

Since photosensitizer specific delivery, transport, and spatial distribution within tumor tissues are all affected by multiple physicochemical and biological factors, the development of strategies that allow active tumor targeting are essential for improving their biological efficacy.[9] Several strategies have been investigated aimed at improving the selective delivery of porphyrin sensitizers to tumor tissues; most of these involve the conjugation of photosensitizers to carrier proteins,[10−12] oligonucleotides,[13,14] monoclonal antibodies (mAb),[15,16] and peptide sequences directed against antigens or ligands that are overexpressed on cancer cells (e.g., EGFR).[17,18] Of particular relevance to drug delivery is the use of peptides containing signaling sequences, such as a NLS[19] or CPP[a],[20−24] where the rational integration of these targeting entities increases the drug pharmacologic concentrations within tumor tissues. CPPs based on the HIV-1 Tat basic domain sequence, GRKKRRQRRR, have been used to deliver a wide range of compounds to targeted cells, including proteins,[25,26] peptides,[27] antisense oligonucleotides,[28,29] liposomes,[30] and 40 nm magnetic iron nanoparticles,[31,32] and have also been shown to penetrate the blood−brain barrier (BBB).[33] Other CPPs based on the *Drosophilia* homeotic

* To whom correspondence should be addressed. Phone: 225-578-9764. Fax: 225-578-9895. E-mail: isehgal@vetmed.lsu.edu.

[a] Abbreviations: CPP, cell penetrating peptide; NLS, nuclear localizing signal; PSA, prostate specific antigen; HOBt, 1-hydroxybenzotriazole; TFA, trifluoroacetic acid; DIEA, *N,N*-diisopropylethylamine; TBTU, 2-(1*H*-benzotriazole-1-yl)-1,1,3,3-tetramethyluronium tetrafluoroborate; Boc, *t*-butoxy carbonyl; HEPES, 4-(2-hydroxyethyl)-1-piperazine ethanesulfonic acid; PBS, phosphate buffered saline; FBS, fetal bovine serum; DMEM: Dulbecco's modified Eagle's medium; PEG, polyethylene glycol; TIS, triisopropylsilane.

10.1021/jm800444c CCC: $40.75
Published on Web 09/11/2008

Scheme 1. Structures of Porphyrin−Peptide Conjugates **1**−**5**

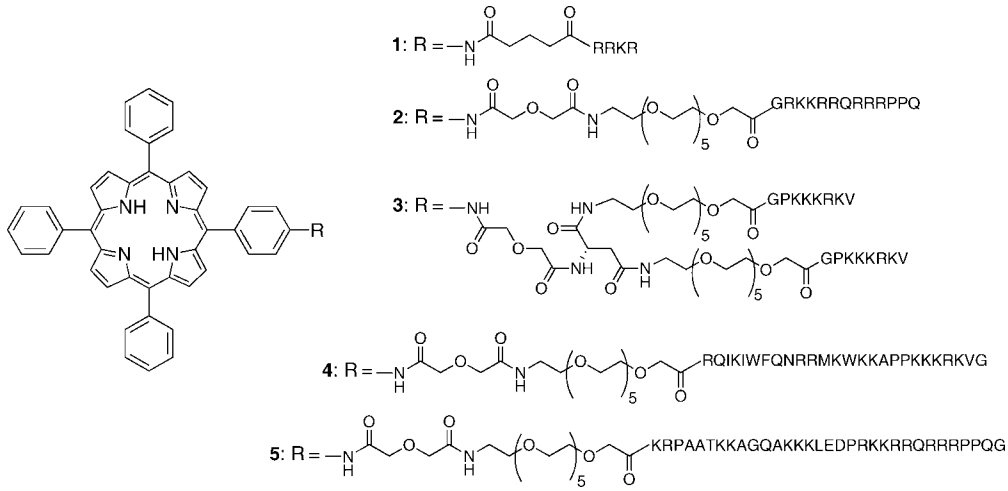

transcription protein antennapedia [penetratin, Antp (43−58)] sequence, RQIKIWFQNRRMKWKK, have been also investigated.[34] The use of NLS represents another useful strategy for targeted drug delivery to the highly vulnerable cell nuclei.[19] In particular, the sequence PKKKRKV derived from the simian virus 40 (SV40) large T antigen,[35] and the minimal sequence KRPAATKKAGQAKKKL from nucleoplasmin,[35,36] are the best characterized. Porphyrin derivatives bearing the NLS SV40 have been reported by us, and in all cases, these conjugates showed increased photosensitizing activity in comparison with the corresponding unconjugated porphyrins.[37] Although in vitro studies of porphyrin sensitizers conjugated to peptides containing a CPP (HIV-1 Tat or penetratin) have shown significantly increased cellular uptake and phototoxicity compared with unconjugated porphyrin,[37−39] the use of peptides as drug carriers in vivo has been limited due in part to their susceptibility to enzymatic hydrolysis and apparently lack of tumor specificity.[40−42] As a consequence, only a few studies have appeared in the literature regarding the in vivo biological efficacy of porphyrin−peptide conjugates, e.g. ref 43. In the present study, we investigated the photosensitizing ability of five porphyrin−peptide conjugates toward PC-3M human prostate cancer cells in vitro in comparison with FDA-approved purified hematoporphyrin derivative and the second generation PDT photosensitizer, mTHPC. The PC-3M prostate cancer cell was chosen because it represents an advanced, androgen-independent prostate cancer, which readily forms tumors in vivo with moderate growth rate.[44,45] The most promising conjugate was further evaluated in an in vivo biodistribution study using SCID mice bearing PC-3M tumors, in comparison with purified hematoporphyrin derivative. Our results show that the cell targeted porphyrin−HIV-1 Tat conjugate is significantly more selective for PC-3M prostate tumors than purified hematoporphyrin derivative and induces much higher phototoxicity in PC-3M cells than either purified hematoporphyrin derivative or mTHPC.

2. Results and Discussion

2.1. Synthesis and Characterization. We synthesized five model porphyrin−peptide conjugates containing either a short 4 cationic amino acid sequence (**1**), a CPP (**2**), two NLS (**3**), or a single bifunctional CPP-NLS (**4**) or NLS-CPP (**5**) peptides, linked by either a short five-carbon or a low molecular weight PEG linkage (Scheme 1). Conjugate **1** was previously shown to have relatively high uptake in human carcinoma HEp2 cells and to preferentially adopt a bent bundle-type conformation as a result of its short porphyrin−peptide linkage.[46] On the other hand, the porphyrin−HIV 1 Tat (48−60) conjugate **2** showed the highest uptake in human carcinoma HEp2 cells of a series of conjugates bearing either a CPP or NLS linked via a short PEG spacer.[37] Furthermore, we have also shown that a boronated porphyrin conjugated to the HIV-1 Tat (48−60) sequence via a PEG linkage also shows significantly higher uptake than the nonconjugated porphyin.[38] The new di-NLS branched conjugate **3** was prepared using a similar strategy from 5-(*p*-aminophenyl)-10,15,20-triphenylporphyrin by initial reaction with diglycolic anhydride[37] followed by coupling with di-Boc protected aspartic acid using HOBt and EDCI and deprotection with TFA. The resulting dicarboxylate terminated porphyrin reacted with protected $NH_2CH_2CH_2(OCH_2CH_2)_5OCH_2CO_2{}^tBu$ in the presence of HOBt and TBTU[37] and after deprotection using TFA and final coupling to HGlyProLys(Boc)Lys(Boc)Lys(Boc)Arg(Pbf)Lys(Boc)Val(O^{t}Bu), followed by deprotection with TFA/TIS/H_2O/phenol 88/2/5/5, conjugate **3** was obtained in 25% overall yield. Porphyrins **4** and **5** bearing a single bifunctional CPP-NLS or NLS-CPP sequence, respectively, have both shown high cellular uptake by human HEp2 cells and were prepared as we have previously reported.[42] All conjugates were purified by reverse phase HPLC and characterized using MS, UV−vis, ^{1}H NMR, and in the case of conjugates **2**−**5**, also by CD. The CD results suggest that all conjugates with the exception of **1** adopt extended rather than bent conformations, probably as a result of the presence of the PEG linker and the electrostatic repulsion between the cationic amino acids on the peptide sequences.[37,42]

2.2. Cell Culture Studies. The five porphyrin conjugates **1**−**5**, FDA-approved purified hematoporphyrin derivative, and the second generation photosensitizer mTHPC, were evaluated in PC-3M human prostate cancer cells in vitro and the results obtained are shown in Figures 1–3 and in Table 1. All conjugates accumulated within PC-3M cells to a significantly higher extent that purified hematoporphyrin derivative and mTHPC (Figure 1). These results are in agreement with our previous studies showing that porphyrin−peptide conjugates generally show increased cellular uptake compared with nonconjugated porphyrins, in particular those containing CPP peptides.[37−39] Interestingly, the porphyrin−HIV-1 Tat conjugate **2** was the only porphyrin−peptide conjugate showing similar uptake kinetics to both purified hematoporphyrin derivative and mTHPC, steadily accumulating over time up to the 24 h period investigated. Furthermore, conjugate **2** was taken up by PC-

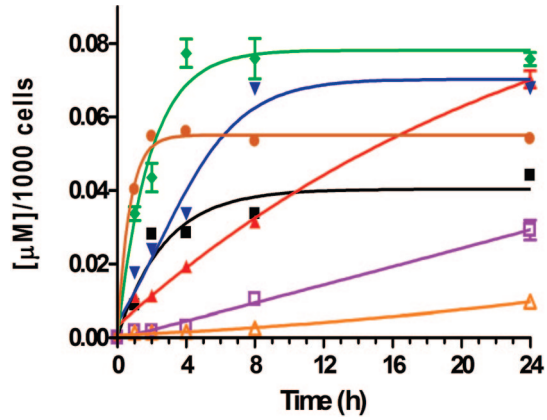

Figure 1. Time-dependent uptake of porphyrin conjugates **1** (green, diamonds), **2** (red, triangles), **3** (brown, circles), **4** (blue, inverted triangles), **5** (black, squares), mTHPC (purple, open squares), and purified hematoporphyrin derivative (orange, open triangles) at 10 μM by PC-3M prostate cancer cells.

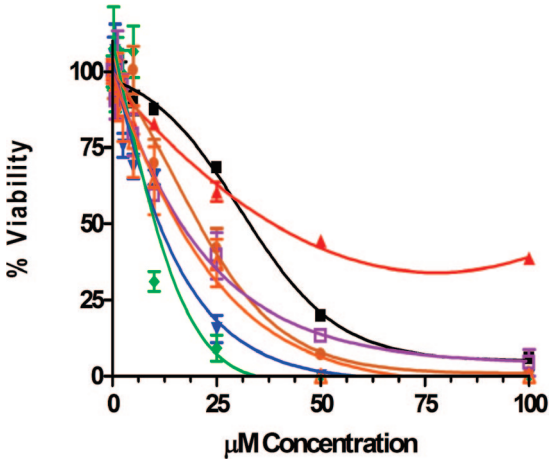

Figure 2. Dark toxicity of porphyrin conjugates **1** (green, diamonds), **2** (red, triangles), **3** (brown, circles), **4** (blue, inverted triangles), **5** (black, squares), mTHPC (purple, open squares), and purified hematoporphyrin derivative (orange, open triangles) toward PC-3M cells using the Cell Titer Blue assay.

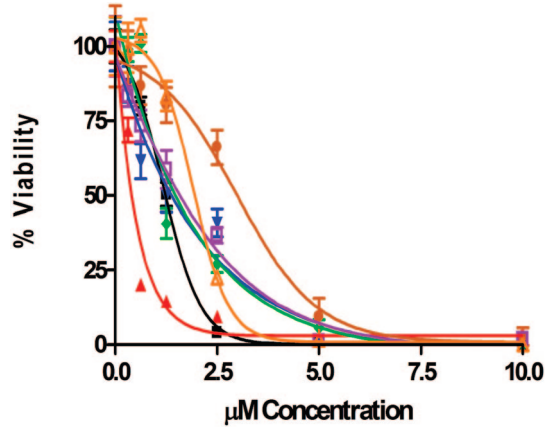

Figure 3. Phototoxicity of porphyrin conjugates **1** (green, diamonds), **2** (red, triangles), **3** (brown, circles), **4** (blue, inverted triangles), **5** (black, squares), mTHPC (purple, open squares), and purified hematoporphyrin derivative (orange, open triangles) toward PC-3M cells using 1 J/cm^2 dose light.

3M cells 5−8 times more than purified hematoporphyrin derivative, at all time points studied. On the other hand, conjugates **1**, **3**, **4**, and **5** were rapidly taken up by cells in the first 2−4 h, after which a plateau was reached and no more conjugate seemed to be internalized after 4−8 h of exposure to cells. Of all conjugates, **1** was found to accumulate the most within PC-3M cells at times longer than 2 h. After 24 h, similar amounts of conjugates **1**, **2**, and **4** were found within cells. It is interesting to note that of the two conjugates bearing the bifunctional sequences (i.e., **4** and **5**), the one containing the CPP-NLS rather than the NLS-CPP peptide showed significantly higher accumulation in PC-3M cells in contrast to the results obtained using human carcinoma HEp2 cells.[42] Furthermore, although conjugate **5** also contains the HIV-1 Tat (48−60) sequence, it accumulated within PC-3M cells to a lower extent than **1**, **3**, and **4**, and after 24 h it was the least found in cells of all porphyrin−peptide conjugates investigated. Our studies show that the cellular uptake of porphyrin−peptide conjugates does not only depend on the nature of the peptide sequences and the linker used but also on the type of cells being targeted. In particular, purified hematoporphyrin derivative showed comparatively low uptake by PC-3M prostate cancer cells, the lowest of all porphyrins tested.

Of all porphyrins investigated, the porphyrin−HIV-1 Tat (48−60) conjugate **2** was the least toxic to PC-3M prostate cells in the dark (IC_{50} = 38 μM) and the most phototoxic upon activation with low light dose (1 J/cm^2 light, IC_{50} = 0.4 μM), as shown in Figures 2 and 3 and in Table 1. Conjugates **1** and **4** showed the highest dark toxicity (IC_{50} = 11 μM) and similar light-induced toxicity to that of mTHPC. On the other hand the di-NLS branched conjugate **3** showed similar dark toxicity to purified hematoporphyrin derivative and mTHPC, but it was significantly less phototoxic. It is interesting to note that this conjugate was the least phototoxic to PC-3M cells of all porphyrins investigated although it contains two SV40 NLS peptides. In contrast to these findings, we have previously observed that a SV40-containing porphyrin conjugate was more phototoxic to human carcinoma HEp2 cells than the corresponding HIV-1 Tat (48−60) porphyrin conjugate.[37] Porphyrin **5**, bearing a bifunctional NLS-CPP linear peptide containing the HIV-1 Tat (48−60) sequence, was also found to be more phototoxic to PC-3M cells and to have significantly lower dark toxicity than either purified hematoporphyrin derivative or mTHPC, although it was less phototoxic than **2**. Of all porphyrins tested, conjugate **2** had the highest IC_{50}(dark)/IC_{50}(light) ratio (96) while purified hematoporphyrin derivative, mTHPC, and conjugates **1**, **3**−**5** all had small ratios between 7 and 27. Our results indicate that substantial photodynamic cytotoxicity can be induced in human prostate cancer cells using porphyrin−peptide conjugate **2** at levels corresponding with minimal dark toxicity. Furthermore, because conjugate **2** showed favorable cellular uptake by PC-3M cells (Figure 1), 5−8 times higher than either purified hematoporphyrin derivative or mTHPC at all time points investigated, it was selected as the most promising photosensitizer to be evaluated for intracellular localization and in an in vivo biodistribution study (vide infra).

The intracellular porphyrin fluorescence of the most promising porphyrin−HIV-1 Tat conjugate **2** was visualized by fluorescence microscopy after exposure of PC-3M cells to 10 μM of this conjugate for 16 h. Conjugate **2** appears to localize solely intracellularly rather than pericellularly, although we have not ruled out its possible accumulation in the tumor vasculature or other aspects of the microenvironment, as has been reported for other porphyrin-type PDT agents.[32] The subcellular localization of conjugate **2** was examined by comparison with nuclear, mitochondrial, lysosomal, and endoplasmic reticulum (ER)

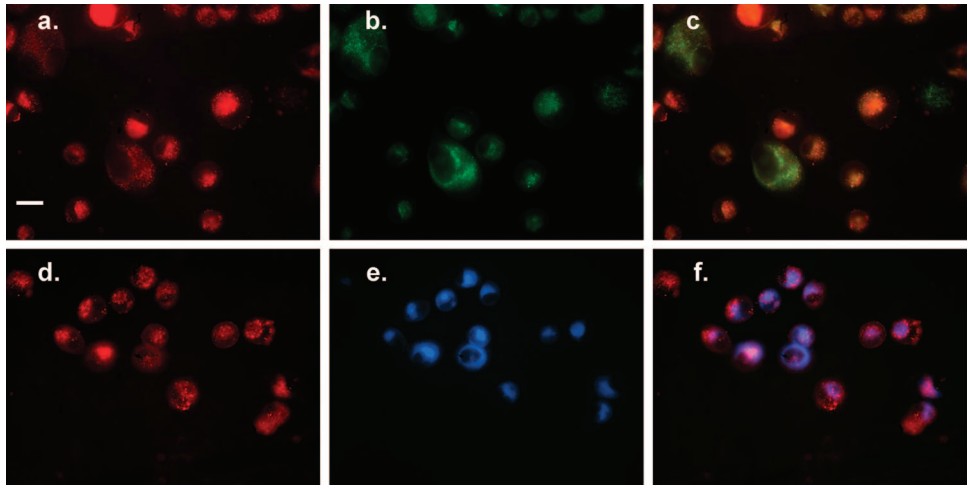

Figure 4. Subcellular localization of conjugate **2**. (a), (d) Red fluorescence indicating location of conjugate **2**. (b) Green fluorescence indicating location of lysosomes in cells from (a). (c) Overlay of (a) with (b). (d) Red fluorescence of conjugate **2** location. (e) Blue fluorescence indicating location of (ER) in cells from (d). (f) Overlay of (d) with (e). The degree of orange (in (c)) or purple (in (f)) color indicates the intensity of conjugate **2** and organelle colocalization in individual cells. Scale bar: 25 μm.

Table 1. Determined IC_{50} Values for Dark and Photoinduced Toxicity of Porphyrin−Peptide Conjugates **1**−**5**, Purified Hematoporphyrin Derivative, and mTHPC toward PC-3M Cells

porphyrin	**1**	**2**	**3**	**4**	**5**	mTHPC	purified hematoporphyrin derivative
dark IC_{50} (μM)	10.7	38.3	20.8	11.4	32.9	16.1	15.4
light (~1 J/cm^2) IC_{50} (μM)	1.48	0.40	2.95	1.34	1.21	1.61	1.95

probes. No colocalization was found in the nucleus or mitochondria (data not shown). Conjugate **2** appears to accumulate mainly in the lysosomes and ER (Figure 4), as we have previously shown in human carcinoma HEp2 cells.[37] In fact, the majority of porphyrin−peptide conjugates that we have previously synthesized and investigated localize within the lysosomes,[37,38,42,46] possibly as a result of an endocytic mechanism of uptake. Both the lysosomes and ER are important targets for the PDT-induced initiation of apoptosis,[47,48] which may in part explain the observed phototoxicity of these conjugates.

2.3. Animal Biodistribution Study. The most promising porphyrin−peptide conjugate **2** (readily taken up by PC-3M cancer cells in vitro, with minimal dark toxicity but potent phototoxicity) was further evaluated in an in vivo biodistribution study using male SCID mice bearing PC-3M tumors, in comparison with FDA-approved purified hematoporphyrin derivative. The mice were administered with a 1.0 μmol/kg body weight dose of either conjugate **2** or purified hematoporphyrin derivative via ip injection. The tissues were collected after 24 h, assayed by ex vivo fluorescence, and the results obtained are shown in Table 2 (each number represents the mean ± standard error for 4 mice). Conjugate **2** showed a highly favorable distribution pattern, appearing limited primarily to the liver and tumor tissues and accumulated to a significantly higher extent than purified hematoporphyrin derivative at the same drug dose within prostate tissue. A precise tumor/blood and tumor/skin ratio could not be calculated because the residues in the blood and skin were not detectable. Porphyrin photosensitizers are often found in the liver in addition to the tumor due to the high amount of reticuloendothelial cells in this organ. The lack of uptake of conjugate **2** by the normal mouse prostate further suggests that the chemistry of this photosensitizer is tumor, rather than prostate, selective. On the other hand, purified hematoporphyrin derivative was detected in the liver, spleen, lung, and blood in addition to the tumor, and in all of these, the amount of purified hematoporphyrin derivative was higher than in tumor. These results suggest a much weaker specific affinity of purified hematoporphyrin derivative for the tumor cells compared with **2**, in agreement with our observations in the PC-3M prostate tumor cells in vitro. In particular, the high levels of purified hematoporphyrin derivative found in blood indicate a far less selective biodistribution in comparison with **2**. In fact, the existence of purified hematoporphyrin derivative in the blood after 24 h suggests that it is cleared more slowly than conjugate **2**, although we have not evaluated the pharmacokinetic elimination rate in this study. Neither porphyrin was detectable in the skin where unwanted dermal phototoxicity has been commonly reported to occur in PDT, suggesting that skin photosensitivity might not be an undesirable side effect in the PDT treatment of prostate tumors.

3. Experimental Section

3.1. Chemistry. Unless otherwise indicated, all commercially available starting materials were used directly without further purification. NMR spectra were obtained on a Varian INOVA-500 instrument. Chemical shifts (δ) are given in ppm relative to TMS. Electronic absorption spectra were measured on a Perkin-Elmer Lambda 35 UV−vis spectrophotometer. Mass spectra were obtained on a Bruker ProFLEX III MALDI-TOF mass spectrometer with a MALDI ionization source using CCA as the matrix. HPLC separation and analysis were performed on a Dionex system including a P680 pump and UVD340U detector. Semipreparative HPLC was carried out using a Luna C_{18} 100 Å, 5 μm, 10 mm × 250 mm (Phenomenex, USA) column and a stepwise gradient; analytical HPLC was carried out using a Delta Pak C_{18} 300 Å, 5 μm, 3.9 mm × 150 mm (Waters, USA) column and a stepwise gradient. The linear porphyrin−peptide conjugates **1**,[46] **2**,[37] **4**,[42] and **5**[42] were synthesized as we have previously described. Photofrin and mTHPC were kindly provided by Prof. Giulio Jori, University of Padova, Italy.

3.1.1. Porphyrin−Peptide Conjugate 3. This conjugate was synthesized from 5-(*p*-aminophenyl)-10,15,20-triphenylporphyrin by reaction with diglycolic anhydride, as we have previously reported.[37] The resulting carboxylate terminated porphyrin (0.100 g, 0.134 mmol) was dissolved in 1 mL of DMF and to this solution were added in the following order: Et_3N (0.012 g, 0.122 g), HOBt (0.186 g, 0.122 mmol), aspartic acid di-*t*-butyl ester hydrochloride

Table 2. Tissue Biodistribution of Conjugate **2** and Purified Hematoporphyrin Derivative after Drug Administration[a]

porphyrin	liver	kidney	tumor	prostate	spleen	lung	skin	blood
2	16.1 ±1.1[a]	≤bkgd	8.1 ±2.4	≤bkgd	≤bkgd	≤bkgd	≤bkgd	≤bkgd
purified hematoporphyrin derivative	8.7 ±0.63	≤bkgd	2.6 ±0.40	≤bkgd	5.5 ± 2.4	4.4 ± 0.90	≤bkgd	12.5 ± 3.3

[a] Data expressed as pmol/mg protein; ≤ bkgd = quantity detected was equal to or below background reading for the porphyrin.

(0.034 g, 0.122mmol), and EDCI (0.023 g, 0122 mmol). The reaction mixture was stirred at room temperature for 48 h before being diluted with ethyl acetate (25 mL) and washed with water (3 × 25 mL). The organic phase was dried over Na_2SO_4, filtered, and the solvent evaporated under vacuum to give a purple residue, which was purified by flash chromatography on silica gel using dichloromethane/methanol 9:1 for elution (0.117 g, 98% yield). UV−vis ($CHCl_3$) λ_{max} (ε/M^{-1} cm^{-1}) 419 (491700), 516 (19700), 551 (10400), 590 (7400), 646 (5800). ^{1}H NMR ($CDCl_3$, 300 MHz): δ 8.97−9.04 (8H, m), 8.22−8.36 (10H, m), 7.79−7.82 (10H, m), 4.93−4.99 (1H, m), 4.49 (2H, s), 4.43 (2H, s), 2.90−3.16 (4H, m), 1.59 (18H, s), −2.59 (2H, s). ^{13}C NMR ($CDCl_3$, 75 MHz): 170.60, 169.50, 168.32, 166.94, 142.08, 137.01, 135.01, 134.48, 131.09, 127.65, 126.62, 120.13, 118.38, 82.80, 81.99, 71.35, 71.03, 48.72, 37.21, 28.02, 27.89. HRMS (MALDI) *m/z* 973.4310 (M + H^+), calculated for $C_{60}H_{57}N_6O_7$ 973.4289. The Boc-protected carboxylate was dissolved in 5 mL of TFA, the reaction mixture was stirred at room temperature 4 h, and then the solvent was evaporated under vacuum to leave a green residue. The solid residue was washed with diethyl ether (5 × 10 mL) and dried under vacuum to give the corresponding dicarboxylate terminated porphyrin intermediate (0.088 g, 99% yield). UV−vis ($CHCl_3$) λ_{max} (ε/M^{-1} cm^{-1}) 420 (228500), 516 (15700), 552 (8000), 590 (5200), 646 (4000). ^{1}H NMR (d_6, DMSO, 300 MHz): δ 10.49 (2H, s), 8.80−8.88 (8H, m), 8.48−8.51 (2H, d), 8.17−8.22 (10H, m), 7.81 (10H, s) 4.71−4.78 (1H, m), 4.38 (2H, s), 4.26 (2H, s), 2.67−2.93 (2H, m). ^{13}C NMR (d_6, DMSO, 75 MHz): 172.28, 171.90, 169.11, 168.32, 158.54, 158.14, 141.06, 134.97, 134.47, 131.15, 128.25, 127.13, 120.12, 118.29, 117.20, 70.85, 70.44, 48.33, 35.99. HRMS (MALDI) *m/z* 861.3006 (M + H^+), calculated for $C_{52}H_{41}N_6O_7$ 861.3037. This compound (0.030 g, 0.035 mmol) was dissolved in 600 μL of DMF, to this solution were added in the following order: DIEA (0.036 g, 0.278 mmol), HOBt (0.0344 g, 0.087 mmol), TBTU (0.028 g, 0.087 mmol), and $NH_2CH_2CH_2(OCH_2CH_2)_5CH_2CO_2{}^tBu$ (0.034 g, 0.087 mmol). The reaction mixture was stirred at room temperature 48 h, then diluted with EtOAc (20 mL), the organic phase washed with water (2 × 20 mL), saturated $NaHCO_3$ (2 × 20 mL), water (2 × 20 mL), dried over Na_2SO_4, filtered, and the solvent evaporated under vacuum to leave a purple residue. The title compound was separated by flash chromatography on silica gel using dichloromethane, dichloromethane/methanol 95/5, and dichloromethane/methanol 90/10 for elution. (0.033 g, 59% yield). UV−vis ($CHCl_3$) λ_{max} (ε/M^{-1} cm^{-1}) 414 (406000), 512 (16900), 547 (9,000), 589 (5400), 645 (4100). ^{1}H NMR ($CDCl_3$, 300 MHz): δ 8.62−8.90 (8H, m), 8.17−8.24 (10H, m), 7.73−7.80 (9H, m), 7.34 (1H, s), 7.11 (1H, s), 4.83−4.87 (1H, m), 4.36 (2H, s), 4.30−4.31 (2H, d, J = 3 Hz), 4.04 (2H, s), 3.99 (2H, s), 3.49−3.71 (48H, m), 2.94−3.01 (1H, dd, J = 4.24, 2.94 Hz), 2.62−2.69 (1H, dd, J = 5.52, 2.62), 1.47 (9H, s), 1.45 (9H, s), −2.75 (2H, s). ^{13}C NMR ($CDCl_3$, 75 MHz): 171.54, 169.63, 168.79, 142.09, 134.38, 134.49, 127.68, 126.65, 120.09, 118.75, 81.51, 70.45, 68.93, 50.01, 39.54, 28.05. HRMS (MALDI) *m/z* 1615.7897 (M^+), calculated for $C_{88}H_{110}N_8O_{21}$ 1615.7818. Boc-protected pegylated porphyrin (0.033 g, 0.020 mmol) was dissolved in 1 mL of DCM, and to this solution was added TFA (1 mL). The reaction mixture was stirred at room temperature 4 h, and then the solvent evaporated under vacuum to leave a green residue. The solid residue was washed with Et_2O to remove traces of TFA and then dried under vacuum (0.030 g, 98% yield). UV−vis ($CHCl_3$) λ_{max} (ε/M^{-1} cm^{-1}) 420 (233600), 516 (11900), 552 (6700), 590 (5000), 647 (4100). ^{1}H NMR ($CDCl_3$, 300 MHz): δ 9.78 (2H, s), 9.23 (8H, s), 8.59−8.61 (8H, m), 8.43−8.45 (2H, d, J = 6.69 Hz), 8.00−8.03 (9H, m), 7.81 (1H, s), 7.74 (1H, s), 5.00−5.02 (1H, m), 4.49 (2H, s), 4.41 (2H, s), 4.12−4.18 (4H, m), 3.53−3.67 (48H, m), 2.88−3.06 (2H, m). HRMS (MALDI) *m/z* 1525.6453 (M + Na^+), calculated for $C_{80}H_{94}N_8O_{21}Na$ 1525.6431. Pegylated porphyrin (0.030 g, 0.020 mmol) was dissolved in 1 mL of DMF, and to this solution were added Et_3N (0.020 g, 0.20 mmol), HOBt (0.007 g, 0.044 mmol), DMAP (0.0005 g, 0.0044 mmol), and HGlyProLys(Boc)Lys(Boc)Lys(Boc)Arg(Pbf)Lys(Boc)Val(O^tBu) (0.082 g, 0.05 mmol). The reaction mixture was stirred at room temperature 48 h. Work up was performed as described above. The porphyrin-protected peptide conjugate was isolated by flash chromatography on silica gel using $CHCl_3$:MeOH 9:1, 8:2 for elution. Yield 0.045 g, 48%. UV−vis ($CHCl_3$) λ_{max} (ε/M^{-1} cm^{-1}) 414 (406000), 512 (16900), 547 (9000), 589 (5400), 645 (4100). ^{1}H NMR ($CDCl_3$, 300 MHz): δ 8.84−8.81 (6H, m), 8.14−8.22 (8H, m), 7.73−7.81 (8H, m), 4.29−4.39 (8H, m), 4.01 (5H, s), 3.40−3.69 (45H, m), 2.93−3.06 (15H, m), 2.17−2.51 (15H, m), 2.04 (10H, s), 1.12−1.78 (134H, m), 0.93 (12H, s), −2.98 (2H, s). LRMS (MALDI) *m/z* M/3 1588.70, calculated for $C_{238}H_{364}N_{38}O_{59}S_2$ M = 4762.6092, M/3 = 1588.5364. The porphyrin-protected peptide conjugate (0.040 g, 0.008 mmol) was dissolved in 2 mL of a mixture TFA/TIS/H_2O/phenol 88/2/5/5. The reaction mixture was stirred at room temperature 4 h, then the solvent evaporated under vacuum to leave a green oily residue. The deprotected conjugate was precipitated by the addition of Et_2O. The green precipitate was washed with Et_2O (5 × 10 mL) and then dried under vacuum. Yield 0.025 g, 95%. HPLC t_r = 12.73 min. UV−vis (MeOH) λ_{max} (ε/M^{-1} cm^{-1}) 415 (283500), 513 (13000), 548 (7700), 588 (5500), 645 (4600). ^{1}H NMR (D_2O, 400 MHz): δ 8.68−8.70 (3H, m), 8.29−8.31 (3H, m), 8.13−1.14 (8H, m), 7.18−7.31 (1H, m), 6.88−6.97 (1H, m), 3.95−4.42 (27H, m), 3.63−3.71 (67H, m), 4.46−3.49 (8H, m), 3.19−3.21 (7H, m), 2.86 (24H, s), 1.44−2.11 (84H, m), 0.89−0.96 (12H, m). LRMS (MALDI) *m/z* M/3 1116.10, calculated for $C_{164}H_{252}N_{38}O_{37}$ M = 3345.9006, M/3 = 1116.3002.

3.2. Cell Culture. All tissue culture media and reagents were obtained from Invitrogen. Human prostate PC-3M cells were a gift from Dr. Isaiah Fidler (UT M. D. Anderson Cancer Center, Houston, TX) and maintained in DMEM supplemented with 10% FBS. The cells were subcultured biweekly to maintain subconfluent stocks.

3.2.1. Time-Dependent Cellular Uptake. PC-3M prostate cancer cells were seeded at 10000 cell/cm^2 in 24-well plates in DMEM high-glucose media with 10% FBS and allowed to attach overnight. The cells were incubated with 10 μM (prepared from a 10 mM stock solution) of each conjugate for various time periods up to 24 h. At the end of the uptake periods, the wells were washed with PBS and the cells were solubilized using 1.0 mL of 0.25% Triton-X. The conjugate concentration (expressed as μM/1000 cells) was determined by fluorescence emission using a SynergyHT-1 plate reader (360 nm excitation/645 nm emission). A known conjugate concentration with the cells was used to standardize the fluorescence readings, and the cell numbers were obtained from duplicate treated plates.

3.2.2. Dark Cytotoxicity. Prostate cancer cells plated as above were exposed to increasing porphyrin conjugate concentrations up to 100 μM and incubated for 24 h in quadruplicate wells. The wells were then washed to remove detached cells and debris. We characterized the material that was detached after exposure to the porphyrin conjugates to confirm that it was nonviable by using a differential fluorescent staining technique (Apoalert Annexin V-EGFP Apoptosis kit, BD-Bio Sciences). We found that this material was overwhelmingly (>99.5%) nonviable, composed of approximately 92% necrotic cells and 8% membrane debris. Cells remaining attached to the wells were removed via trypsinization, and viable cells were enumerated using a hemocytometer. Control wells consisting of cells not treated with porphyrins were also counted, and these control cell numbers were set at 100% viability. Data points are expression of the viability of porphyrin-treated cells as a percentage of controls.

3.2.3. Phototoxicity. PC-3M cells plated as above were exposed to increasing porphyrin conjugate concentrations for 24 h in quadruplicate wells. After this period, the porphyrin conjugates were removed by thorough washing with PBS and the media was replaced with DMEM buffered with HEPES (50 mM, pH 7.4). The cells were placed in an ice bath and exposed to light from a 100 W halogen lamp filtered through a 610 nm long pass light filter for 20 min. An inverted plate lid filled with water acted as an infrared filter. The total light dose was approximately 1 J/cm^2. The cells were then incubated overnight and enumerated as for dark toxicity above.

3.2.4. Intracellular Localization. PC-3M cells plated onto glass chamber slides were exposed to 10 μM of conjugate **2** over a 16 h period for uptake and intracellular distribution. Cell cultures were then supplemented with organelle markers for endoplasmic reticulum (ER-Tracker Blue-White DPX, Molecular Probes, Eugene, OR, used at 2 mM final concentration), lysosomes (LysoSensor DND-189, Molecular Probes, Eugene, OR, used at 50 nM final concentration), mitochondria (MitoTracker Green FM, Molecular Probes, Eugene, OR, used at 250 nM final concentration), or nucleus (4′,6-diamidino-2-phenylindole (DAPI), Sigma Chemicals, St. Louis, used at 1 μg/mL final concentration) for 30 min. Following incubation, the cells were washed 3 times with PBS and live-imaged using a Zeiss Axiovert 200 fluorescence microscope fitted with a Texas Red filter set (to capture porphyrin conjugate fluorescence), an FITC filter set (to capture MitoTracker and LysoSensor probes), and a DAPI-compatible filter set (to capture DAPI as well as ER-Tracker probes). Images were captured using a Retiga 2000R digital camera at 400× magnification, and data is presented for organelles that appeared to contain the conjugate (lysosomes and ER).

3.4. Animal Studies. Male SCID mice at 8 weeks of age were purchased from Jackson laboratories (Bar Harbor, Maine) and were housed in an ALAC-approved facility. All experiments conformed to protocols approved by the LSU-SVM IACUC.

3.4.1. Tumor System. PC-3M prostate cancer cells (2×10^6 cells per mouse) were sterilely injected into the dorsum of the back between the shoulder blades. Tumors were allowed to form over a 5−6 week period. When tumors attained a size of approximately 0.1 cm^3 (calculated as length × width × depth × 0.5), mice were administered porphyrins at a dosage of 1.0 μmol/kg body weight ip in a 5% dextrose solution (as per Photofrin package insert).

3.4.2. Porphyrin Biodistribution. Twenty-four hours after porphyrin administration, the following tissues were collected as ≅ 5 mm × 5 mm × 5 mm samples: tumor, skin, lung, liver, spleen, kidney, and prostate. Blood (60−70 μL) was also collected. All tissue sections were incubated in 0.6 mL ScintiGest solubilization solution (Fisher Scientific) at 37 °C for 24 h then homogenized using a Teflon pestle (Thomas Scientific) rotated on a bench drill press (Ryobi DP-101) and returned to incubation overnight. Following centrifugation to remove insoluble material, supernatants were analyzed using a SynergyHT-1 fluorescence plate reader at 530 nm (absorption)/645 nm (emission). Fluorescence readings of tissue extracts were quantitated using KC4 software and were based on a four-parameter equation generated from a standard curve of each porphyrin dissolved in Scintigest solution mixed with different tissues assayed. Final data are expressed as pmol porphyrin/mg tissue protein after subtraction of nonspecific fluorescence. This background fluorescence for each tissue was measured using mice injected with vehicle-only.

4. Conclusions

We have examined a series of five porphyrin−peptide conjugates in vitro using PC-3M human prostate cells and compared their performance with FDA-approved purified hematoporphyrin derivative and to a structurally related second-generation PDT photosensitizer, mTHPC. Among these photosensitizers, we identified a highly promising porphyrin−HIV-1 Tat conjugate **2** for the PDT treatment of human prostate cancer, that showed low dark cytotoxicity, high phototoxicity (IC_{50} = 0.40 μM at 1 J/cm^2), IC_{50}(dark)/IC_{50}(light) = 96, and favorable in vitro cellular uptake and in vivo biodistribution. In comparison with FDA-approved purified hematoporphyrin derivative, this porphyrin−CPP conjugate is less toxic in the dark toward PC-3M cells, is significantly more phototoxic, and accumulates to a significantly higher extent within tumor cells both in vitro and in vivo. Furthermore, the porphyrin−HIV-1 Tat conjugate **2** is significantly more prostate tumor selective than purified hematoporphyrin derivative, which unlike **2** was also detected in several normal tissues in addition to the tumor and in high levels in blood. Conjugate **2** was also found to accumulate to a higher extent within PC-3M cells in vitro and to be less toxic in the dark and significantly more phototoxic than mTHPC, a second-generation photosensitizer that has shown promise in the PDT treatment of prostate tumors. Our results indicate that the coupling of a long-wavelength absorbing porphyrin photosensitizer to the HIV-1 Tat (48−60) sequence might lead to enhanced PDT of prostate tumors and/or tumor tomography.

Acknowledgment. We thank Martha Juban for peptide sequence syntheses, Dr. Thomas K. Weldeghiorghis for NMR data acquisition, and Timothy Jensen for assistance in optimizing culture assays. This work was partially supported by the National Science Foundation, grant number CHE-304833, and by a Competitive Organized Research Program grant from the LSU-SVM to I.S.

Supporting Information Available: The ^{1}H NMR and HPLC trace for the new porphyrin conjugate **3** are provided. This material is available free of charge via the Internet at http://pubs.acs.org.

References

(1) Dougherty, T. J.; Gomer, C. J.; Henderson, B. W.; Jori, G.; Kessel, D.; Korbelik, M.; Moan, J.; Peng, Q. Photodynamic Therapy. *J. Natl. Cancer Inst.* **1998**, *90*, 889–905.

(2) Pandey, R. K.; Zheng, G. Porphyrins as photosensitizers in photodynamic therapy. In *The Porphyrin Handbook*; Kadish, K. M., Smith, K. M., Guilard, R., Eds.; Academic Press: Boston, 2000; Vol. 6, pp 157−230.

(3) Brown, S. B.; Brown, E. A.; Walker, I. The present and future role of photodynamic therapy in cancer treatment. *Lancet Oncol.* **2004**, *5*, 497–508.

(4) Du, K. L.; Mick, R.; Busch, T. M.; Zhu, T. C.; Finlay, J. C.; Yu, G.; Yodh, A. G.; Malkowicz, S. B.; Smith, D.; Whittington, R.; Stripp, D.; Hahn, S. M. Preliminary results of interstitial motexafin lutetium-mediated PDT for prostate cancer. *Lasers Surg. Med.* **2006**, *38*, 427–434.

(5) Pinthyus, J. H.; Bogaards, A.; Weersink, R.; Wilson, B. C.; Trachtenberg, J. Photodynamic therapy for urological malignancies: past to current approaches. *J. Urol.* **2006**, *175*, 1201–1207.

(6) Trachtenberg, J.; Bogaards, A.; Weersink, R. A.; Haider, M. A.; Evans, A.; McCluskey, S. A.; Scherz, A.; Gertner, M. R.; Yue, C.; Appu, S.; Aprikian, A.; Savard, J.; Wilson, B. C.; Elhilali, M. Vascular targeted photodynamic therapy with palladium-bacteriopheophorbide photosensitizer for recurrent prostate cancer following definitive radiation therapy: Assessment of safety and treatment response. *J. Urol.* **2007**, *178*, 1974–1979.

(7) Nathan, T. R.; Whitelaw, D. E.; Chang, S. C.; Lees, W. R.; Ripley, P. M.; Payne, H.; Jones, L.; Parkinson, M. C.; Emberton, M.; Gillams, A. R.; Mundy, A. R.; Bown, S. G. Photodynamic therapy for prostate cancer recurrence after radiotherapy: a phase I study. *J. Urol.* **2002**, *168*, 1427–1432.

(8) Moore, C. M.; Nathan, T. R.; Lees, W. R.; Mosse, C. A.; Freeman, A.; Emberton, M.; Bown, S. G. Photodynamic therapy using meso tetra hydroxy phenyl chlorin (mTHPC) in early prostate cancer. *Lasers Surg. Med.* **2006**, *38*, 356–363.

(9) (a) Hamblin, M. R.; Newman, E. L. Photosensitizer targeting in photodynamic therapy. I. Conjugates of haematoporphyrin with albumin and transferrin. *J. Photochem. Photobiol. B: Biol.* **1994**, *26*, 45–56. (b) Hamblin, M. R.; Newman, E. L. Photosensitizer targeting in photodynamic therapy. II. Conjugates of haematoporphyrin with serum lipoproteins. *J. Photochem. Photobiol., B* **1994**, *26*, 147–157.

(10) Soini, A. E.; Yashunsky, D. V.; Meltola, N. J.; Ponomarev, G. V. Influence of linker unit on performance of palladium(II) coproporphyrin labelling reagent and its bioconjugates. *Luminescence* **2003**, *18*, 182–192.

(11) Chudinov, A. V.; Rumiantseva, V. D.; Lobanov, A. V.; Chudinova, G. K.; Stomakhin, A. A.; Mironov, A. F. Synthesis of conjugates of bovine serum albumin with water-soluble ytterbium porphyrins. *Bioorg. Khim.* **2004**, *30*, 99104.
(12) Li, H.; Fedorova, O. S.; Trumble, W. R.; Fletcher, T. R.; Czuchajowski, L. Site-specific photomodification of DNA by porphyrin−oligonucleotide conjugates synthesized via a solid phase H-phosphonate approach. *Bioconjugate Chem.* **1997**, *8*, 49–56.
(13) (a) Mestre, B.; Jakobs, A.; Pratviel, G.; Meunier, B. Structure/nuclease activity relationships of DNA cleavers based on cationic metalloporphyrin−oligonucleotide conjugates. *Biochemistry* **1996**, *35*, 9140–9149. (b) Mestre, B.; Pitie, M.; Loup, C.; Claparols, C.; Pratviel, G.; Meunier, B. Influence of the nature of the porphyrin ligand on the nuclease activity of metalloporphyrin−oligonucleotide conjugates designed with cationic, hydrophobic or anionic metalloporphyrins. *Nucleic Acids Res.* **1997**, *25*, 1022–1027.
(14) (a) Del Governatore, M.; Hamblin, M. R.; Piccinini, E. E.; Ugolini, G.; Hasan, T. Targeted photodestruction of human colon cancer cells using charged 17.1A chlorin e_6 immunoconjugates. *Br. J. Cancer* **2000**, *82*, 56–64. (b) Hamblin, M. R.; Del Governatore, M.; Rizvi, I.; Hasan, T. Biodistribution of charged 17.1A photoimmunoconjugates in a murine model of hepatic metastasis of colorectal cancer. *Br. J. Cancer* **2000**, *83*, 1544–1551.
(15) Hudson, R.; Carcenac, M.; Smith, K.; Madden, L.; Clarke, O. J.; Pelegrin, A.; Greenman, J.; Boyle, R. W. The development and characterization of porphyrin isothiocyanate−monoclonal antibody conjugates for photoimmunotherapy. *Br. J. Cancer* **2005**, *92*, 1442–1449.
(16) (a) Gijsens, A.; De Witte, P. Photocytotoxic action of EGF-PVA-Sn(IV)chlorin e6 and EGF-dextran-Sn(IV)chlorin e6 internalizable conjugates on A431 cells. *Int. J. Oncol.* **1998**, *13*, 1171–1177. (b) Gijsens, A.; Missiaen, L.; Merlevede, W.; de Witte, P. Epidermal growth factor-mediated targeting of chlorin e_6 selectively potentiates its photodynamic activity. *Cancer Res.* **2000**, *60*, 2197–2202.
(17) Savitsky, A. A.; Gukasova, N. V.; Gumanov, S. G.; Feldman, N. B.; Luk'yanets, E. A.; Mironov, A. F.; Yakubovskaya, R. I.; Lutsenko, S. V.; Severin, S. E. Cytotoxic action of conjugates of alpha-fetoprotein and epidermal growth factor with photoheme, chlorines, and phthalocyanines. *Biochemistry (Moscow)* **2000**, *65*, 732–736.
(18) Boulikas, T. Nuclear localization signals. *Crit. Rev. Eukaryotic Gene Expression* **1993**, *3*, 193–227.
(19) Richard, J. P.; Melikov, K.; Vives, E.; Ramos, C.; Verbeure, B.; Gait, M. J.; Chernomordik, L. V.; Lebleu, B. Cell-penetrating peptides: a re-evaluation of the mechanism of cellular uptake. *J. Biol. Chem.* **2003**, *278*, 585–590.
(20) Futaki, S.; Goto, S.; Suzuki, T.; Nakase, I.; Sugiura, Y. Structural variety of membrane permeable peptides. *Curr. Protein Pept. Sci.* **2003**, *4*, 87–96.
(21) Snyder, E. L.; Dowdy, S. F. Cell penetrating peptides in drug delivery. *Pharm. Res.* **2004**, *21*, 389–393.
(22) Magzoub, M.; Gräslund, A. Cell-penetrating peptides: small from inception to application. *Q. Rev. Biophys.* **2004**, *37*, 147–195.
(23) Deshayes, S.; Morris, M. C.; Divita, G.; Heitz, F. Cell-penetrating peptides: tools for intracellular delivery of therapeutics. *Cell. Mol. Life Sci.* **2005**, 1839–1849.
(24) Lee, H. J.; Pardridge, W. M. Pharmacokinetics and delivery of Tat and Tat-protein conjugates to tissues in vivo. *Bioconjugate Chem.* **2001**, *12*, 995–999.
(25) Morris, M. C.; Depollier, J.; Mery, J.; Heitz, F.; Divita, G. A peptide carrier for the delivery of biologically active proteins into mammalian cells. *Nat. Biotechnol.* **2001**, *19*, 1173–1176.
(26) Wadia, J.; Dowdy, S. Trans-membrane delivery of protein and peptide drugs by TAT-mediated transduction in the treatment of cancer. *Adv. Drug Delivery Rev.* **2005**, *57*, 579–596.
(27) Oehlke, J.; Birth, P.; Klauschenz, E.; Wiesner, B.; Beyermann, M.; Oksche, A.; Bienert, M. Cellular uptake of antisense oligonucleotides after complexing or conjugation with cell-penetrating model peptides. *Eur. J. Biochem.* **2002**, *269*, 4025–4032.
(28) Lochman, D.; Jauk, E.; Zimmer, A. Drug delivery of oligonucleotides by peptides. *Eur. J. Pharmacol. Biopharmacol.* **2004**, *58*, 237–251.
(29) Torchilin, V. P.; Levchenko, T. S.; Rammohan, R.; Volodina, N.; Papahadjopoulos-Sternberg, B.; D'Souza, G. G. Cell transfection in vitro and in vivo with nontoxic TAT peptide−liposome−DNA complexes. *Proc. Natl Acad. Sci. U.S.A.* **2003**, *100*, 1972–1977.
(30) (a) Becker, M. L.; Remsen, E. E.; Pan, D.; Wooley, K. L. Peptide-derivatized shell-cross-linked nanoparticles. 1. Synthesis and characterization. *Bioconjugate Chem.* **2004**, *15*, 699–709. (b) Becker, M. L.; Bailey, L. O.; Wooley, K. L. Peptide-derivatized shell-cross-linked nanoparticles. 2. Biocompatibility evaluation. *Bioconjugate Chem.* **2004**, *15*, 710–717.
(31) Nitin, N.; LaConte, L.; Zurkiya, O.; Hu, X.; Bao, G. Functionalization and peptide-based delivery of magnetic nanoparticles as an intracellular MRI contrast agent. *J. Biol. Inorg. Chem.* **2004**, *9*, 706–712.
(32) (a) Rouselle, C.; Clair, P.; Smirnova, M.; Kolesnikov, Y.; Pasternak, G. W.; Gac-Breton, S.; Rees, A. R.; Schermann, J. M.; Temsamani, J. Improved brain uptake and pharmacological activity of dalargin using a peptide-vector-mediated strategy. *J. Pharmacol. Exp. Ther.* **2003**, *306*, 371–376. (b) Rouselle, C.; Clair, P.; Temsamani, J.; Schermann, J. M. Improved brain delivery of benzylpenicillin with a peptide-vector-mediated strategy. *J. Drug Targeting* **2002**, *10*, 309–315. (c) Rouselle, C.; Smirnova, M.; Clair, P.; Lefauconnier, J. M.; Chabanieu, A.; Calas, B.; Schermann, J. M.; Temsamani, J. Enhanced delivery of doxorubicin into the brain via a peptide-vector-mediated strategy: saturation kinetics and specificity. *J. Pharmacol. Exp. Ther.* **2001**, *296*, 124–131.
(33) (a) Derossi, D.; Joliot, A.; Chassaing, G.; Prochiantz, A. The third helix of the Antennapedia homeodomain translocates through biological membranes. *J. Biol. Chem.* **1994**, *269*, 10444–10450. (b) Derossi, D.; Calvet, S.; Trembleau, A.; Brunissen, A.; Chassaing, G.; Prochiantz, A. Cell internalization of the third helix of the Antennapedia homeodomain is receptor-independent. *J. Biol. Chem.* **1996**, *271*, 18188–18193.
(34) Kalderon, D.; Roberts, B. L.; Richardson, W. D.; Smith, A. E. A short amino acid sequence able to specify nuclear location. *Cell* **1984**, *39*, 499–509.
(35) (a) Dingwall, C.; Laskey, R. A. Nucleoplasmin: the archetypal molecular chaperone. Semin. *Cell. Biol.* **1990**, *1*, 11–17. (b) Prado, A.; Ramos, I.; Frehlick, L. J.; Muga, A.; Ausio, J. Nucleoplasmin: a nuclear chaperone. *Biochem. Cell Biol.* **2004**, *82*, 437–445.
(36) (a) Akhlynina, T. V.; Jans, D. A.; Rosenkranz, A. A.; Statsyuk, N. V.; Balashova, I. Y.; Toth, G.; Pavo, I.; Rubin, A. B.; Sobolev, A. S. Nuclear targeting of chlorin e_6 enhances its photosensitizing activity. *J. Biol. Chem.* **1997**, *272*, 20328–20331. (b) Akhlynina, T. V.; Jans, D. A.; Statsyuk, N. V.; Balashova, I. Y.; Toth, G.; Pavo, I.; Rosenkranz, A. A.; Naroditsky, B. S.; Sobolev, A. S. Adenoviruses synergize with nuclear localization signals to enhance nuclear delivery and photodynamic action of internalizable conjugates containing chlorin e_6. *Int. J. Cancer* **1999**, *81*, 734–740. (c) Akhlynina, T. V.; Rosenkranz, A. A.; Jans, D. A.; Gulak, P. V.; Serebryakova, N. V.; Sobolev, A. S. The use of internalizable derivatives of chlorin e_6 for increasing its photosensitizing activity. *Photochem. Photobiol.* **1993**, *58*, 45–48.
(37) Sibrian-Vazquez, M.; Jensen, T. J.; Hammer, R. P.; Vicente, M. G. H. Peptide-mediated cell transport of water soluble porphyrin conjugates. *J. Med. Chem.* **2006**, *49*, 1364–1372.
(38) Sibrian-Vazquez, M.; Hao, E.; Jensen, T. J.; Vicente, M. G. H. Enhanced cellular uptake with a cobaltacarborane-porphyrin−HIV-1 Tat 48−60 conjugate. *Bioconjugate Chem.* **2006**, *17*, 928–934.
(39) Chaloin, L.; Bigey, P.; Loup, C.; Marin, M.; Galeotti, N.; Piechaczyk, M.; Heitz, F.; Meunier, B. Improvement of porphyrin cellular delivery and activity by conjugation to a carrier peptide. *Bioconjugate Chem.* **2001**, *12*, 691–700.
(40) Tréhin, R.; Merkle, H. P. Chances and pitfalls of cell penetrating peptides for cellular drug delivery. *Eur. J. Pharmacol. Biopharmacol.* **2004**, *58*, 209–223.
(41) Vives, E. Present and future of cell-penetrating peptide mediated delivery systems: "Is the Trojan horse too wild to go only to Troy?". *J. Controlled Release* **2005**, *109*, 77–85.
(42) Sibrian-Vazquez, M.; Jensen, T. J.; Vicente, M. G. H. Synthesis, characterization, and metabolic stability of water soluble porphyrin−peptide conjugates bearing bifunctional peptide signaling sequences. *J. Med. Chem.* **2008**, *51*, 2915–2923.
(43) Stefflova, K.; Li, H.; Chen, J.; Zheng, G. Peptide-based pharmacomodulation of a cancer-targeted optical imaging and photodynamic therapy agent. *Bioconjugate Chem.* **2007**, *18*, 379–388.
(44) Thomas, S.; Chigurupati, S.; Anbalagan, M.; Shah, G. Calcitonin increases tumorigenicity of prostate cancer cells: evidence for the role of protein kinase A and urokinase-type plasminogen receptor. *Mol. Endocrinol.* **2006**, *20*, 1894–1911.
(45) Giubellino, A.; Gao, Y.; Lee, S.; Lee, M. J.; Vasselli, J. R.; Medepalli, S.; Trepel, J. B.; Bottaro, D. P. Inhibition of tumor metastasis by a growth factor receptor bound protein 2 Src homology 2 domain-binding antagonist. *Cancer Res.* **2007**, *67*, 6012–6016.
(46) Sibrian-Vazquez, M.; Jensen, T. J.; Fronczek, F. R.; Hammer, R. P.; Vicente, M. G. H. Synthesis and characterization of positively charged porphyrin−peptide conjugates. *Bioconjugate Chem.* **2005**, *16*, 852–863.
(47) Linder, S.; Shoshan, M. C. Lysosomes and endoplasmic reticulum: targets for improved, selective anticancer therapy. *Drug Resist. Updates* **2005**, *8*, 199–204.
(48) Tardy, C.; Codogno, P.; Autefage, H.; Levade, T.; Andrieu-Abadie, N. Lysosomes and lysosomal proteins in cancer cell death (new players of an old struggle). *Biochim. Biophys. Acta* **2006**, *1765*, 101–125.

JM800444C